Scaling Geochronologies

Shaun Lovejoy[a], Rhisiart Davies[a] , Andrej Spiridonov[b], Raphael Hebert[c], Fabrice Lambert[d]

[a] Physics, McGill University, 3600 University St., Montreal, Quebec, H2A 3T8, Canada.
[b] Department of Geology and Mineralogy, Faculty of Chemistry and Geosciences, Vilnius University, M. K. Čiurlionio g. 21/27, Vilnius 03101, Lithuania.
[c] Alfred-Wegener Institute Helmholtz Centre for Polar and Marine Research, Telegrafenberg A45, 14473 Potsdam, Germany.
[d] Geography Institute, Pontificia Universitad Catolica de Chile, Vicuña Mackenna 4860, Santiago, Chile.

Supplementary Material

Estimates of α for datasets in the main text

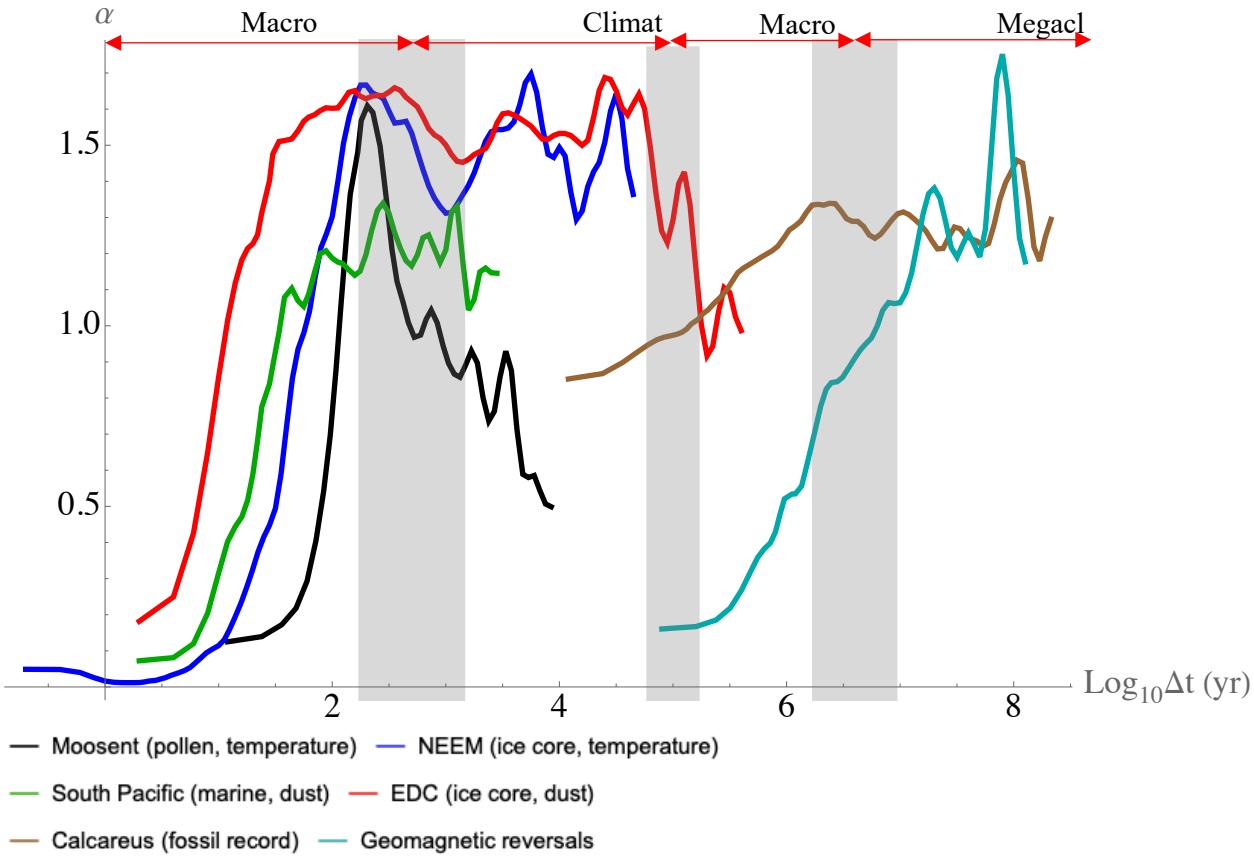

Figure S4: Estimates for the multifractal index α as a function of timescale for all of the representative datasets analysed in the main body of the report. The transition scales between different climate regimes are shown by vertical grey bars. At short time scales, $\alpha \approx 0$, but it undergoes a rapid increase, often at the same timescale at which the scaling regime changes, to reach a plateau of $1 \lesssim \alpha \lesssim 1.5$ at longer timescales. This shows that at short timescales, the measurement density approaches a monofractal set, whereas at longer timescales it appears more as a multifractal.

23 Holocene

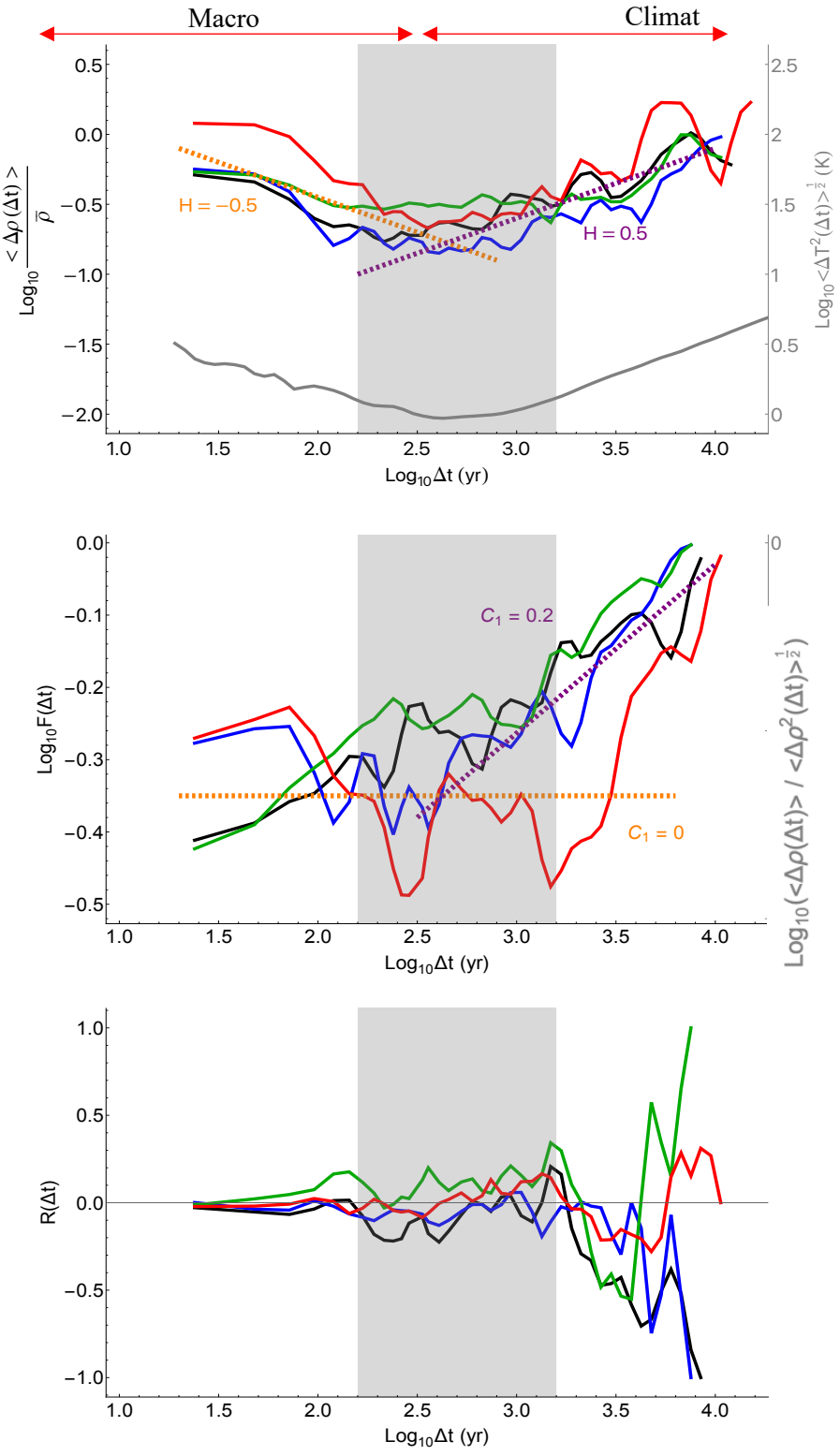

24
25

Figure S5: The results of Haar analysis on datasets that analysed fossilized pollen records over the Holocene. a) $< \rho(\Delta t) >$, the slope of which gives an estimate of H, b) plot of log $F(\Delta t)$, the slope of which gives an estimate of C_1 (and which differs from the log-log plot of the ratio between the fluctuation in measurement density and its root mean square by a constant coefficient for constant α - shown on the right axis), and c) the correlation coefficient between fluctuations in measurement density and fluctuations in the measured quantity. In grey in plot a) are the fluctuations in temperature for the EDC (left) and Grossman (right) datasets to demonstrate the different scaling regimes of the climate system. The transition scale between different climate regimes is shown by a vertical grey bar. Two distinct scaling regimes can be seen: one with $H \approx -0.5$ and $C_1 \approx 0$ (fluctuating sedimentation rate dominant) and a second with $H \approx 0.5$ and $C_1 \approx 0.2$ (erosion process dominant), with a transition timescale around 300 yr.

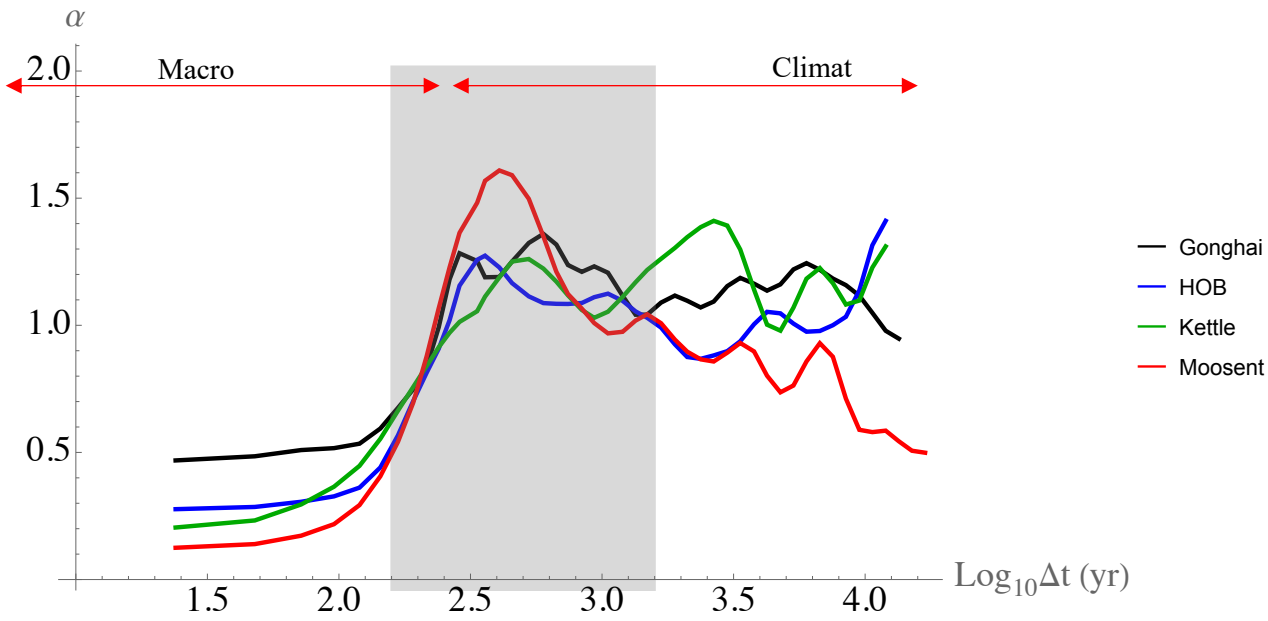

Figure S6: Estimates for the multifractal index α as a function of timescale for datasets that analysed fossilized pollen records over the Holocene. The transition timescale between different climate regimes is shown by a vertical grey bar. At short timescales, $\alpha \approx 0$, but it undergoes a rapid increase - at the same timescale at which the scaling regime changes - to reach a plateau of $1 \lesssim \alpha \lesssim 1.5$ at longer timescales. This shows that at short timescales, the measurement density approaches a monofractal set, whereas at longer timescales it appears more as a multifractal. α for the Moosent dataset does appear to decrease steadily after an initial peak at the transition timescale, however α remains much larger than at the very shortest timescales.

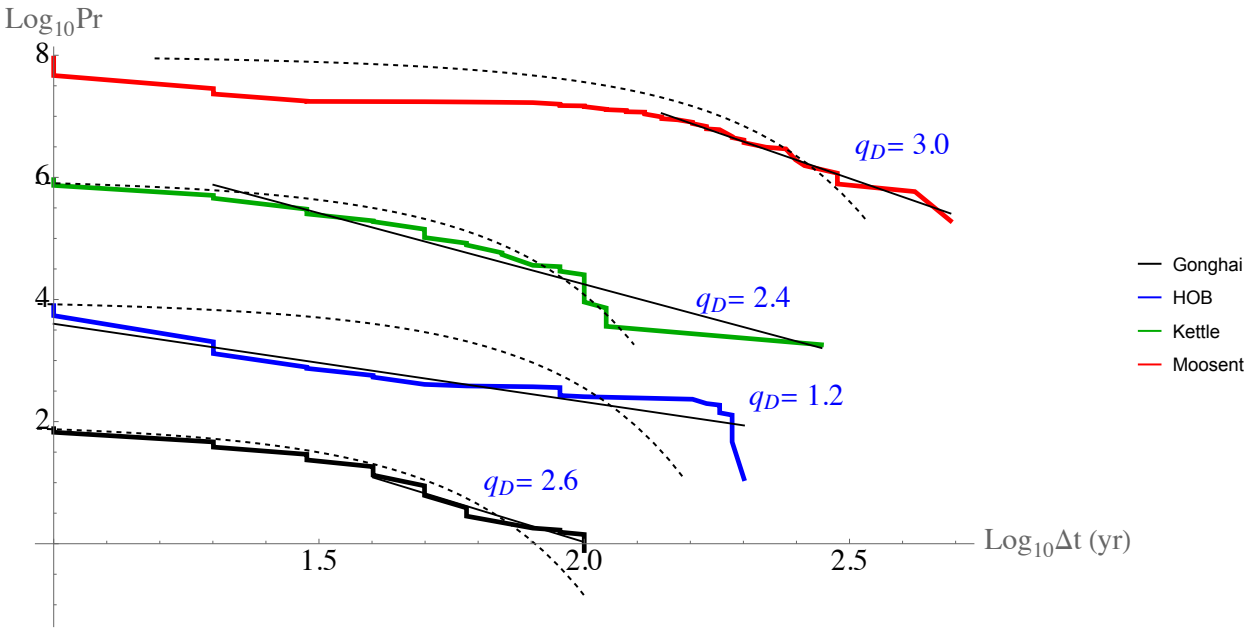

Figure S7: the probability distribution $Pr(\Delta\tau' > \Delta\tau)$ of intervals between consecutive datapoints in the paleo chronologies of datasets that analysed fossilized pollen records over the Holocene, where $\Delta\tau'$ is the duration of a random interval and $\Delta\tau$ is a threshold. Black dotted lines show the best fit Gaussian distribution, whereas straight black lines show a best fit linear curve on a portion of the data. The exponents q_D are shown for the linear log-log fits, where $Pr \approx \Delta\tau^{-q_D}$. Distributions have been offset vertically for presentation. A Gaussian fit does not describe the data sets well, and that all the data sets have long linear tails demonstrating extreme scaling behaviour in the probability distribution, particularly for the HOB dataset with $q_D = 1.2$.

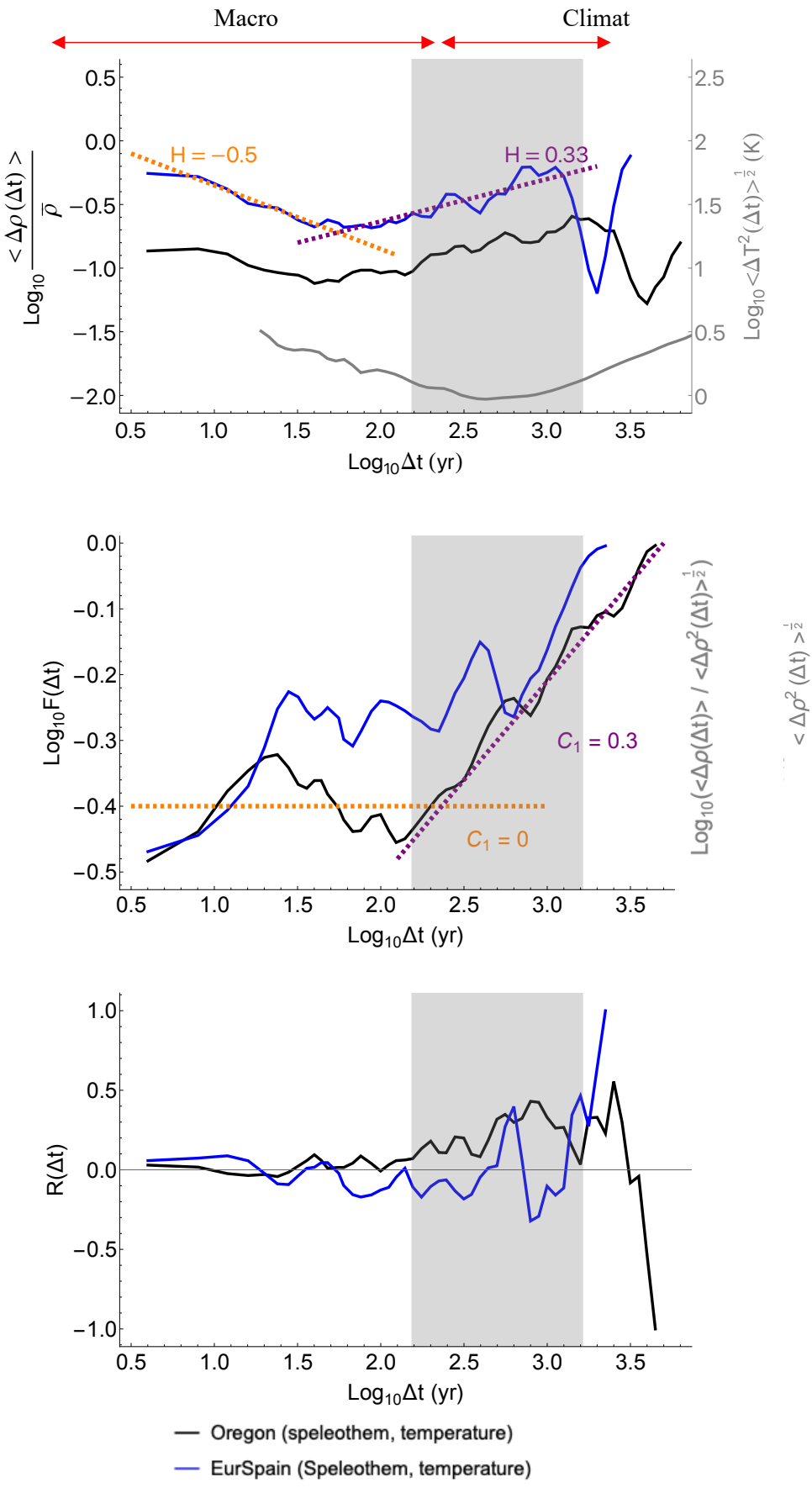
Macro
Climat
H = −0.5
H = 0.33
$\mathrm{Log}_{10}\frac{<\Delta\rho(\Delta t)>}{\bar{\rho}}$
$\mathrm{Log}_{10}<\Delta T^2(\Delta t)>^{\frac{1}{2}}$ (K)
$\mathrm{Log}_{10}\Delta t$ (yr)
$\mathrm{Log}_{10}F(\Delta t)$
$C_1 = 0.3$
$C_1 = 0$
$\mathrm{Log}_{10}(<\Delta\rho(\Delta t)> / <\Delta\rho^2(\Delta t)>^{\frac{1}{2}})$
$<\Delta\rho^2(\Delta t)>^{\frac{1}{2}}$
R(Δt)
Oregon (speleothem, temperature)
EurSpain (Speleothem, temperature)

Figure S8: The results of Haar analysis on datasets that analysed speleothems over the Holocene. a) $< \rho(\Delta t) >$, the slope of which gives an estimate of H, b) plot of log $F(\Delta t)$, the slope of which gives an estimate of C_1, and c) the correlation coefficient between fluctuations in measurement density and fluctuations in the measured quantity. In grey in plot a) are the fluctuations in temperature for the EDC (left) and Grossman (right) datasets to demonstrate the different scaling regimes of the climate system. The transition scale between different climate regimes is shown by a vertical grey bar. Two distinct scaling regimes can be seen: one with $H \approx -0.5$ and $C_1 \approx 0$ (fluctuating sedimentation rate dominant) and a second with $H \approx 0.33$ and $C_1 \approx 0.3$ (erosion process dominant), with a transition timescale or around 100yr.

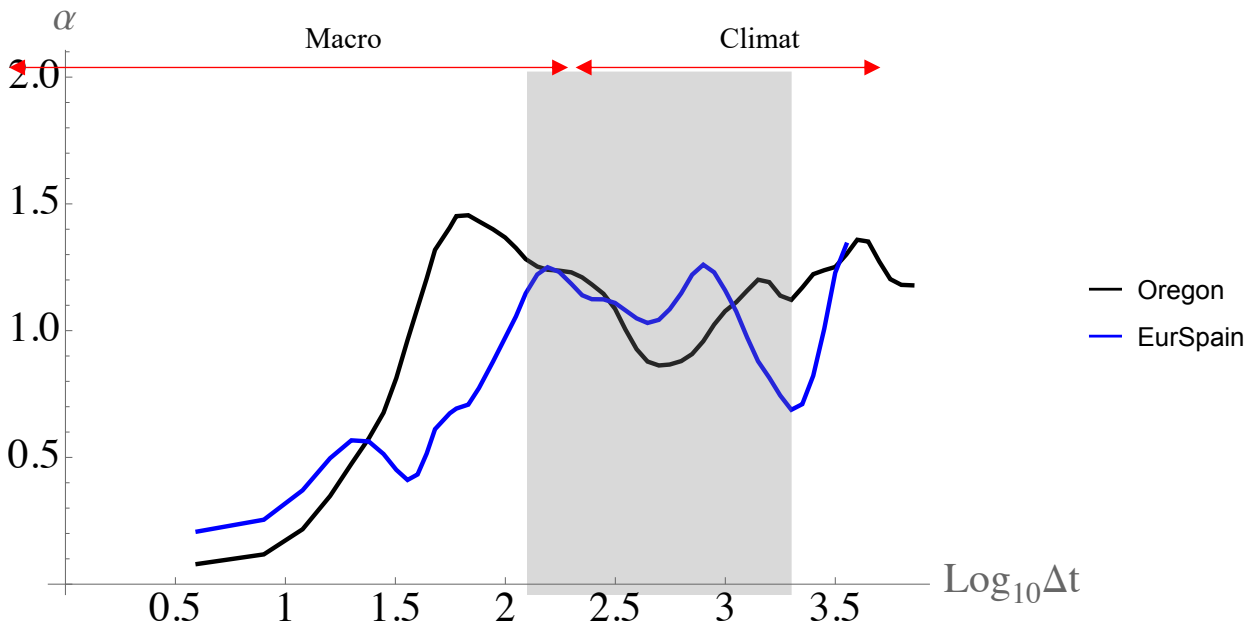

Figure S9: Estimates for the multifractal index α as a function of timescale for datasets that analysed speleothems over the Holocene. The transition timescale between different climate regimes is shown by a vertical grey bar. At short timescales, $\alpha \approx 0$, but it undergoes a rapid increase - at the same timescale at which the scaling regime changes - to reach a plateau of $1 \lesssim \alpha \lesssim 1.5$ at longer timescales. This shows that at short timescales, the measurement density approaches a monofractal set, whereas at longer timescales it appears more as a multifractal.

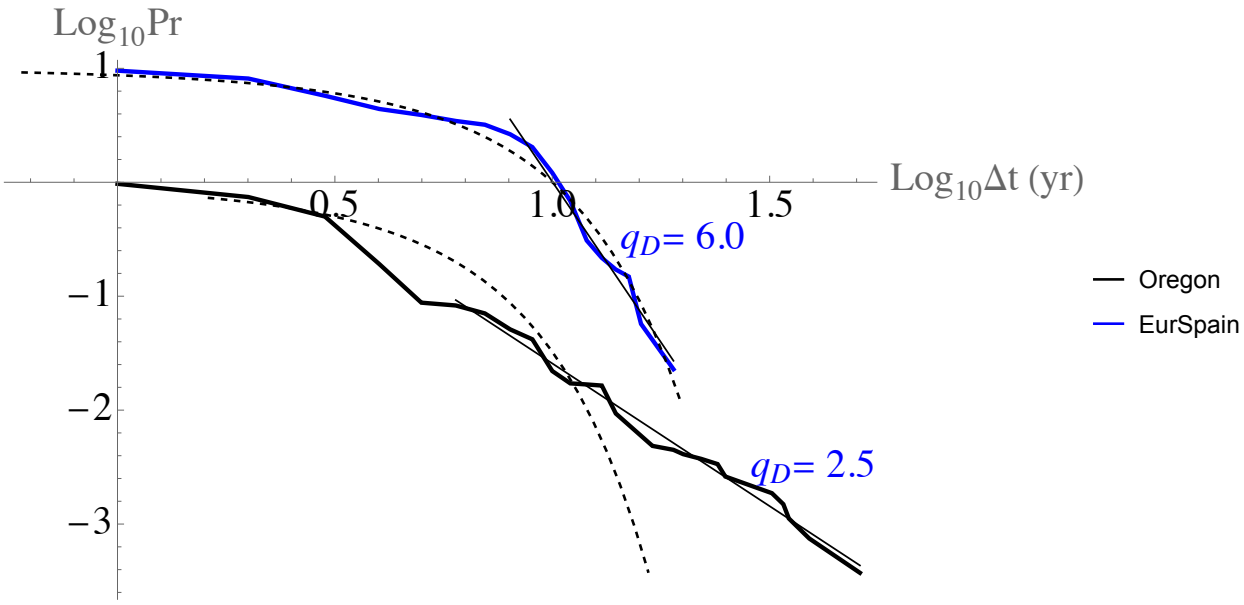

Figure S10: the probability distribution $Pr(\Delta\tau' > \Delta\tau)$ of intervals between consecutive datapoints in the paleo chronologies of datasets that analysed speleothems over the Holocene, where $\Delta\tau'$ is the duration of a random interval and $\Delta\tau$ is a threshold. Black dotted lines show the best fit Gaussian distribution, whereas straight black lines show a best fit linear curve on a portion of the data. The exponents q_D are shown for the linear log-log fits, where $Pr \approx \Delta\tau^{-q_D}$. Distributions have been offset vertically for presentation. A Gaussian fit does not describe the EurSpain data set well, although it describes the Oregon dataset passably at the beginning. Both data sets have linear tails demonstrating scaling behaviour in the probability distribution, although the scaling behaviour of the EurSpain dataset is considerably more extreme than that seen in Oregon.

Quaternary

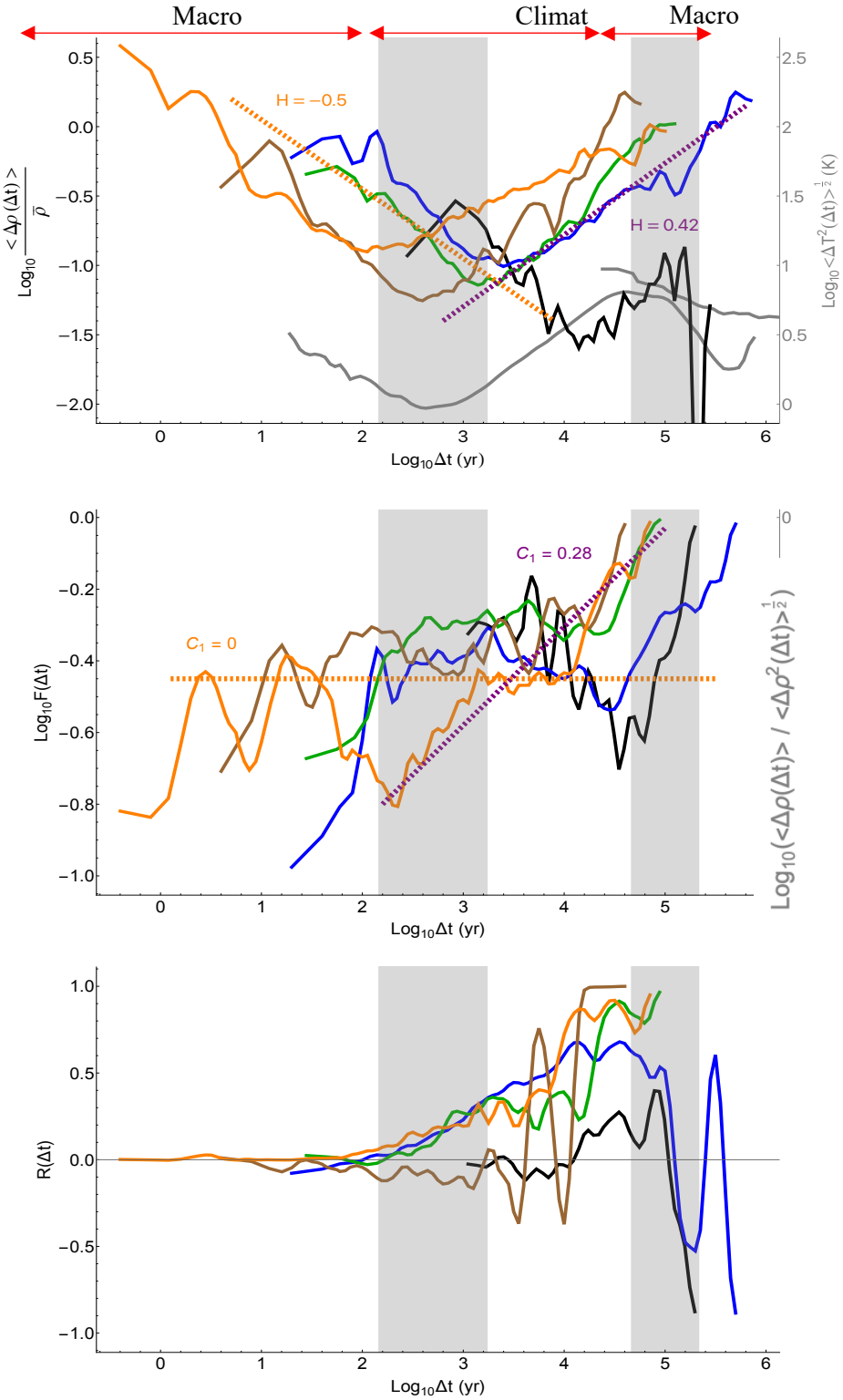

Figure S11: The results of Haar analysis on ice core datasets that measured temperature over the Quaternary. a) $< \rho(\Delta t) >$, the slope of which gives an estimate of H, b) plot of log $F(\Delta t)$, the slope of which gives an estimate of C_1, and c) the correlation coefficient between fluctuations in measurement

density and fluctuations in the measured quantity. In grey in plot a) are the fluctuations in temperature for the EDC (left) and Grossman (right) datasets to demonstrate the different scaling regimes of the climate system. The transition scales between different climate regimes are shown by vertical grey bars. Two distinct scaling regimes can be seen for each dataset: one with $H \approx -0.5$ and $C_1 \approx 0$ (fluctuating sedimentation rate dominant) and a second with $H > 0$ and $C_1 > 0$ (erosion process dominant). There are different transition timescales for the datasets that depend on their latitude. The datasets from the Northern polar regions (WAIS and NEEM) transition at around 100 yr, whereas the datasets from the Southern polar regions (EDC and EDML) transition around 1000 yr. The dataset from mid latitudes (Fuji) transitions at around 10,000 yr.

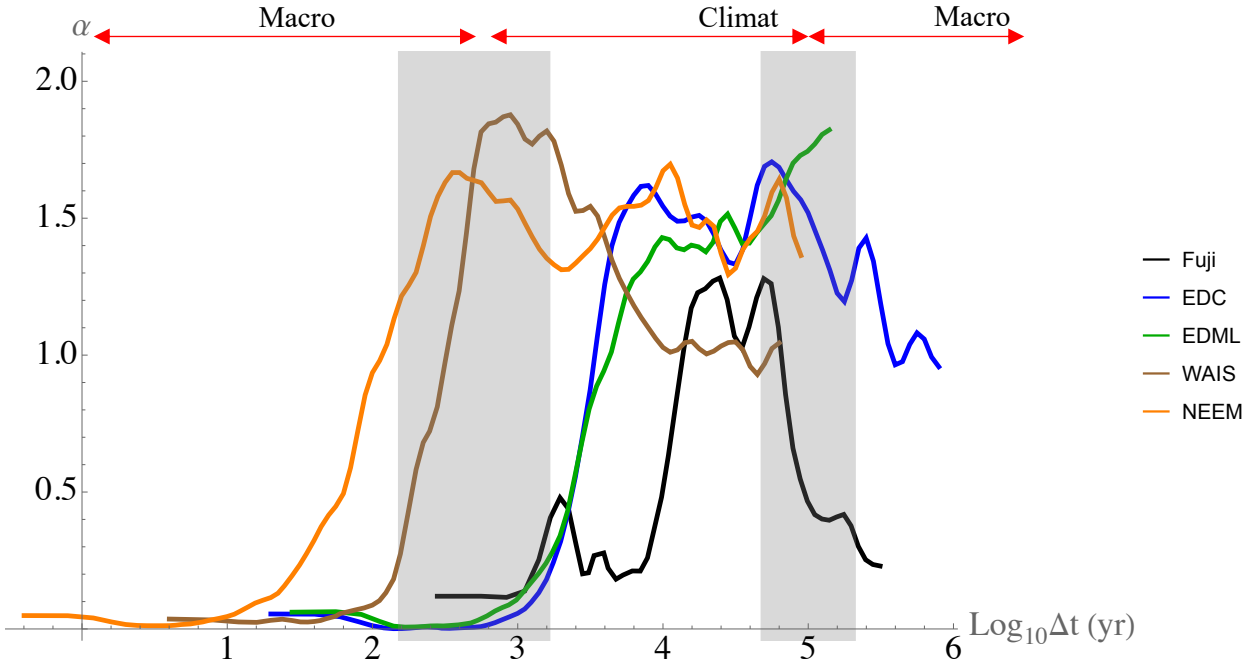

Figure S12: Estimates for the multifractal index α as a function of timescale for ice core datasets that measured temperature over the Quaternary. The transition scales between different climate regimes are shown by vertical grey bars. At short timescales, $\alpha \approx 0$, but it undergoes a rapid increase - at the same timescale at which the scaling regime changes - to reach a plateau of $1 \lesssim \alpha \lesssim 1.5$ at longer timescales. This shows that at short timescales, the measurement density approaches a monofractal set, whereas at longer timescales it appears more as a multifractal. The Fuji dataset does not seem to follow this trend well, as its value for α reaches a peak before decreasing again to values similar to those seen at very high frequencies.

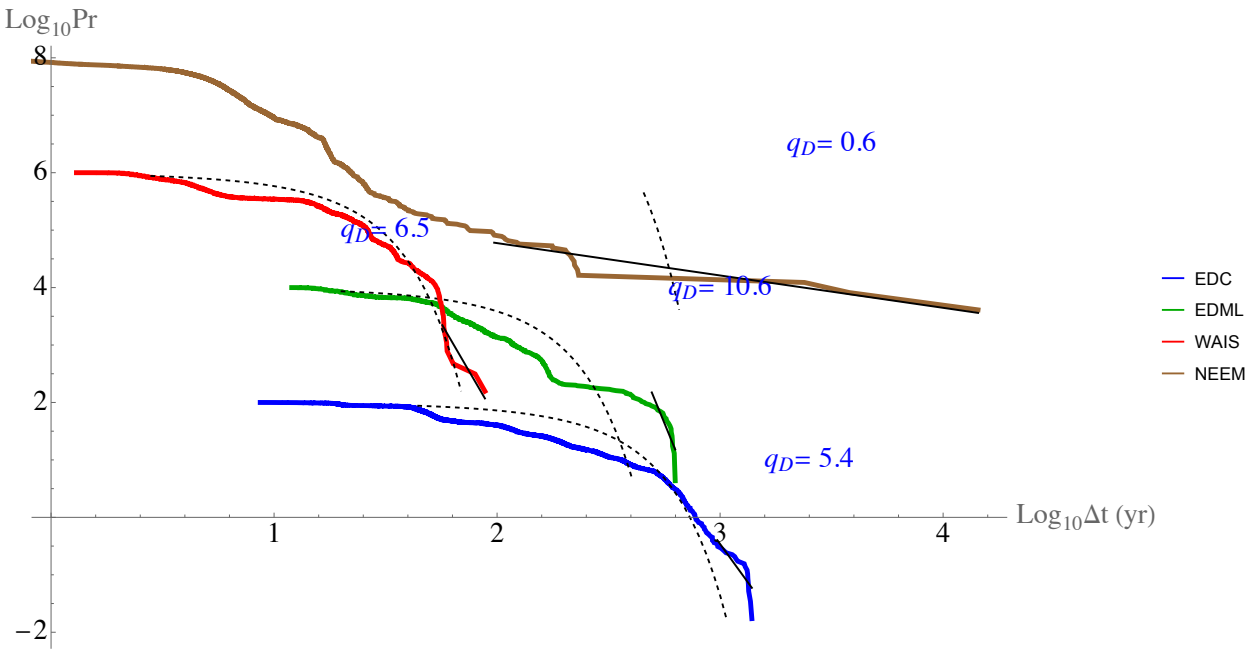

Figure S13: the probability distribution $Pr(\Delta\tau' > \Delta\tau)$ of intervals between consecutive datapoints in the paleo chronologies of datasets that measured temperature over the Quaternary, where $\Delta\tau'$ is the duration of a random interval and $\Delta\tau$ is a threshold. Black dotted lines show the best fit Gaussian distribution, whereas straight black lines show a best fit linear curve on a portion of the data. The exponents q_D are shown for the linear log-log fits, where $Pr \approx \Delta\tau^{-q_D}$. Distributions have been offset vertically for presentation. A Gaussian fit does not describe most of the datasets well, except for the WAIS dataset which roughly follows a Gaussian distribution until the very longest gaps. All the datasets have linear tails demonstrating scaling behaviour in the probability distribution. In particular, the NEEM dataset displays very extreme scaling with $q_D = 0.6$. It should be noted there is no useful probability distribution for the Fuji dataset as it was sampled in such a way that all the times allocated to only had gaps of either 250 yr or 500 yr between them. This means that the measurement density was still free to fluctuate, but the probability distribution only consisted of two values, hence it was not included in this plot.

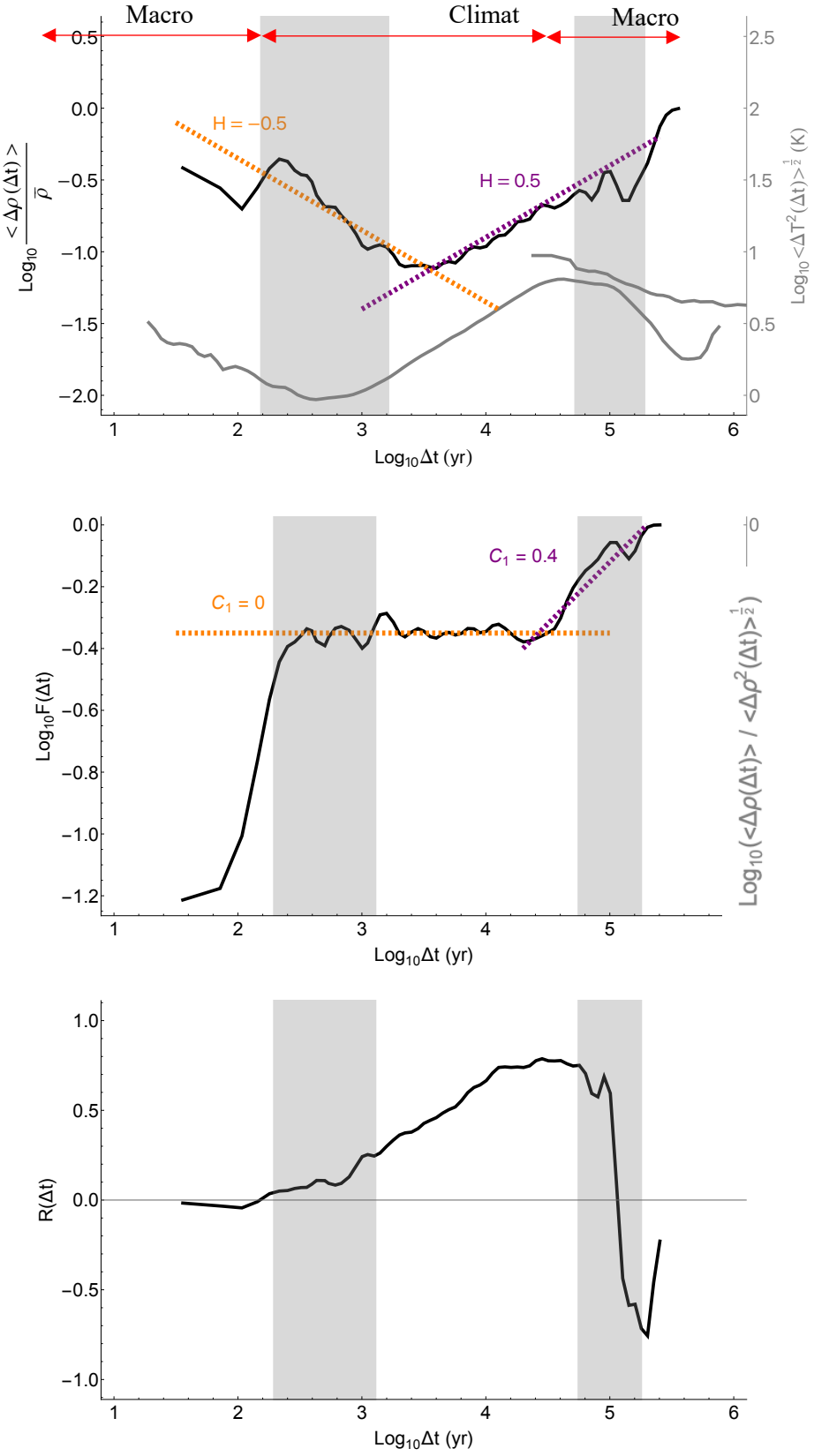
Macro
Climat
Macro
H = −0.5
H = 0.5
$\mathrm{Log}_{10}\frac{<\Delta\rho(\Delta t)>}{\bar{\rho}}$
$\mathrm{Log}_{10}<\Delta T^2(\Delta t)>^{\frac{1}{2}}$ (K)
$\mathrm{Log}_{10}\Delta t$ (yr)
$C_1 = 0$
$C_1 = 0.4$
$\mathrm{Log}_{10}F(\Delta t)$
$\mathrm{Log}_{10}(<\Delta\rho(\Delta t)> / <\Delta\rho^2(\Delta t)>^{\frac{1}{2}})$
$<\Delta\rho(\Delta t)>$
R(Δt)
$\mathrm{Log}_{10}\Delta t$ (yr)

Figure S14: The results of Haar analysis on the Vostok dataset, an ice core that measured temperature anomaly over the Quaternary. a) $< \rho(\Delta t) >$, the slope of which gives an estimate of H, b) plot of log $F(\Delta t)$, the slope of which gives an estimate of C_1, and c) the correlation coefficient between fluctuations in measurement density and fluctuations in the measured quantity. In grey in plot a) are the fluctuations in temperature for the EDC (left) and Grossman (right) datasets to demonstrate the different scaling regimes of the climate system. The transition scales between different climate regimes are shown by vertical grey bars. Two distinct scaling regimes can be seen: one with $H \approx -0.5$ and $C_1 \approx 0$ (fluctuating sedimentation rate dominant) and a second with $H \approx 0.5$ and $C_1 \approx 0.4$ (erosion process dominant). The transition timescale occurs around 3000 yr.

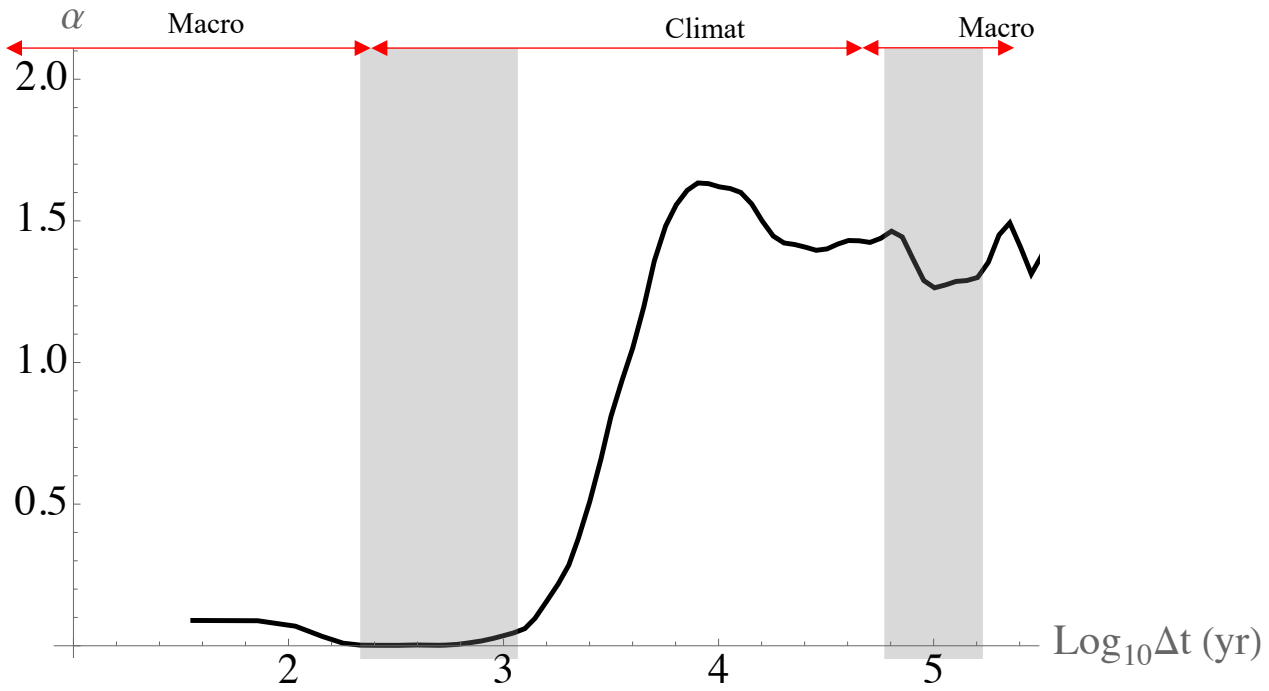

Figure S15: Estimates for the multifractal index α as a function of timescale for the Vostok ice core dataset that measured temperature anomalies over the Quaternary. The transition scales between different climate regimes are shown by vertical grey bars. At short timescales, $\alpha \approx 0$, but it undergoes a rapid increase - at the same timescale at which the scaling regime changes - to reach a plateau of $\alpha \approx 1.4$ at longer timescales. This shows that at short timescales, the measurement density approaches a monofractal set, whereas at longer timescales it appears more as a multifractal.

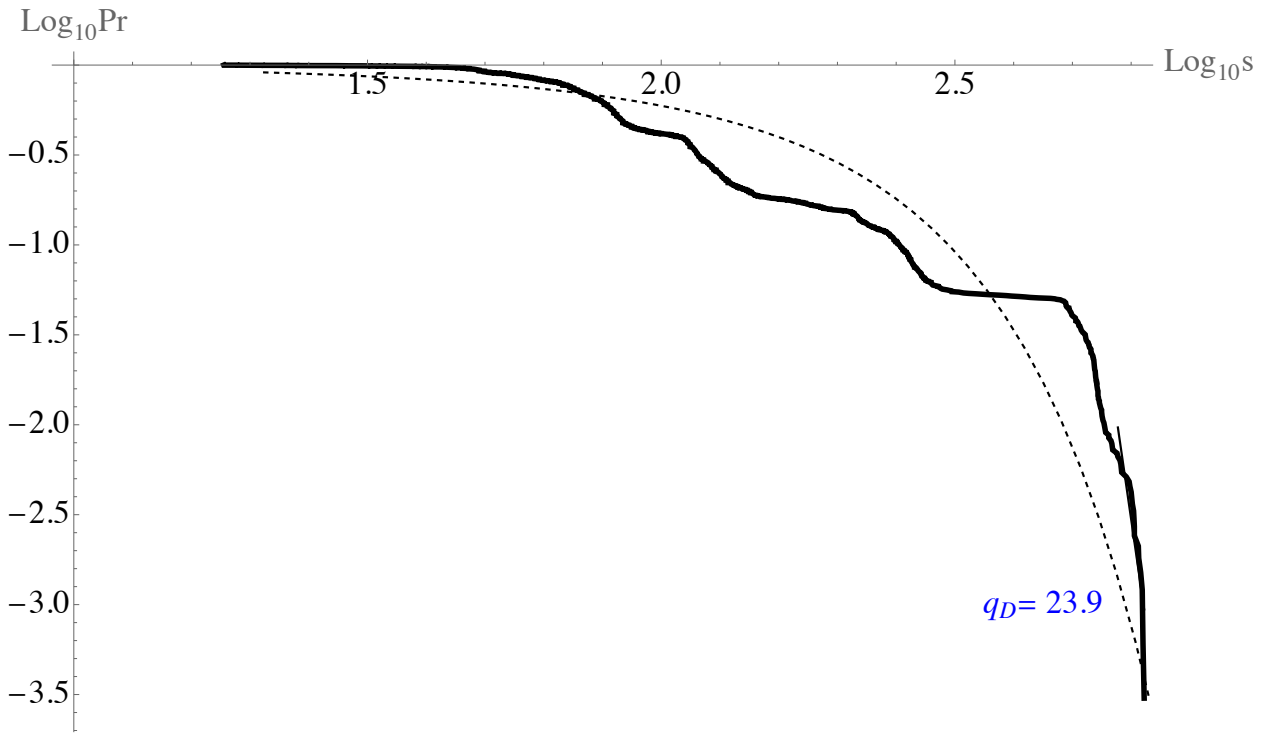

Figure S16: the probability distribution $Pr(\Delta\tau' > \Delta\tau)$ of intervals between consecutive datapoints in the Vostok ice core paleo chronology that measured temperature anomaly over the Quaternary, where $\Delta\tau'$ is the duration of a random interval and $\Delta\tau$ is a threshold. The black dotted line shows the best fit Gaussian distribution, whereas the straight black line shows a best fit linear curve on a portion of the data. The exponent q_D is shown for the linear log-log fit, where $Pr \approx \Delta\tau^{-q_D}$. A Gaussian fit does not describe the dataset well. The dataset has a linear tail with $q_D = 23.9$ demonstrating some scaling behaviour in the probability distribution.

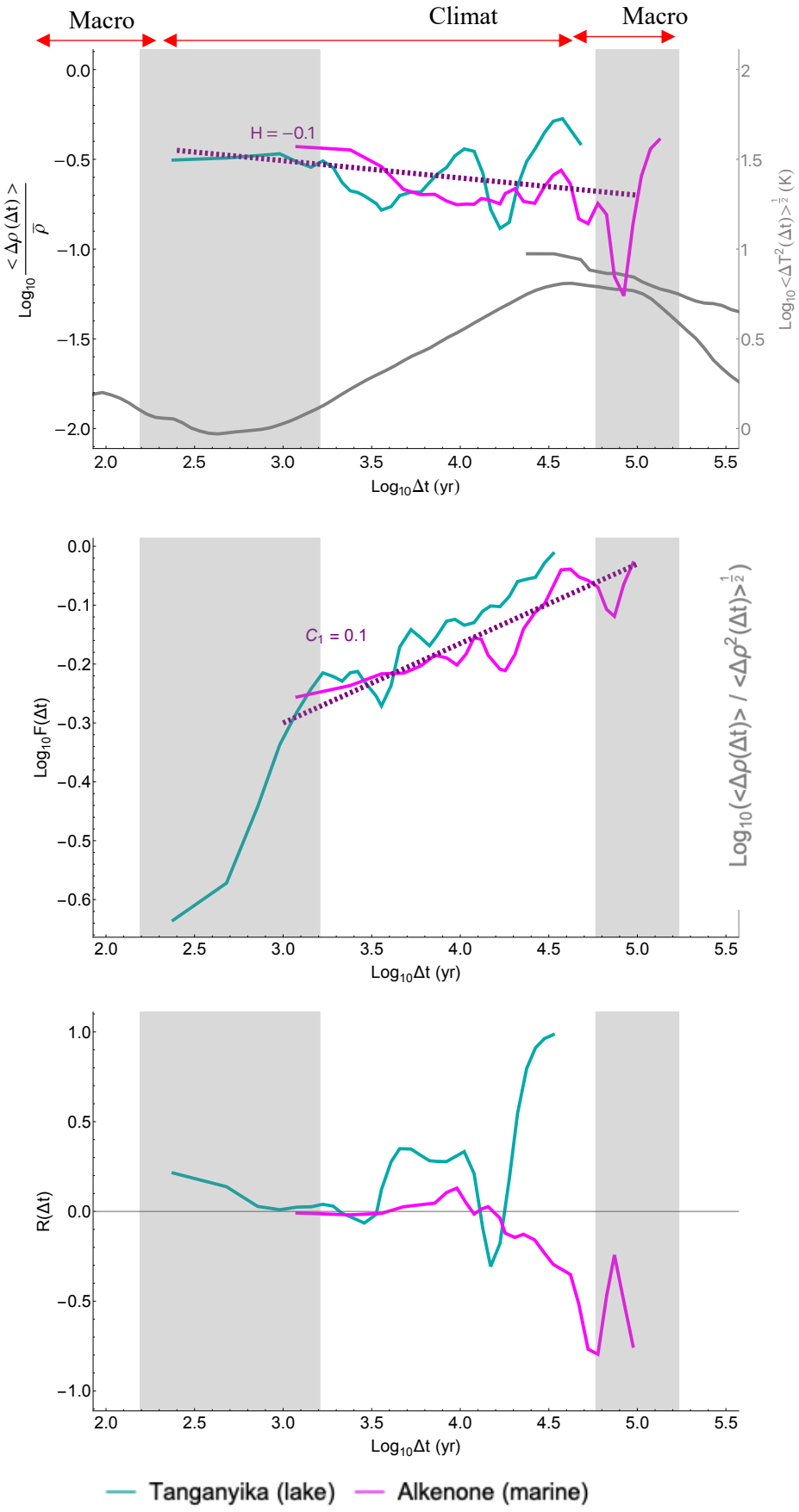
Macro
Climat
Macro
H = −0.1
$\mathrm{Log}_{10}\frac{<\Delta\rho(\Delta t)>}{\bar{\rho}}$
$\mathrm{Log}_{10}<\Delta T^2(\Delta t)>^{\frac{1}{2}}$ (K)
$\mathrm{Log}_{10}\Delta t$ (yr)
C_1 = 0.1
$\mathrm{Log}_{10}F(\Delta t)$
$\mathrm{Log}_{10}(<\Delta\rho(\Delta t)> / <\Delta\rho^2(\Delta t)>^{\frac{1}{2}})$
R(Δt)
Tanganyika (lake)
Alkenone (marine)

Figure S17: The results of Haar analysis on lake and marine sediment datasets that measured temperature over the Quaternary. a) $< \rho(\Delta t) >$, the slope of which gives an estimate of H, b) plot of log $F(\Delta t)$, the slope of which gives an estimate of C_1, and c) the correlation coefficient between fluctuations in measurement density and fluctuations in the measured quantity. In grey in plot a) are the fluctuations in temperature for the EDC (left) and Grossman (right) datasets to demonstrate the different scaling regimes of the climate system. The transition scales between different climate regimes are shown by vertical grey bars. Just one scaling regime can be seen for each dataset with $H \approx -0.1$ and $C_1 \approx 0.1$. This indicates considerable intermittency that is a result of strong erosion processes, yet the measurement density still approaches a well-defined mean regardless.

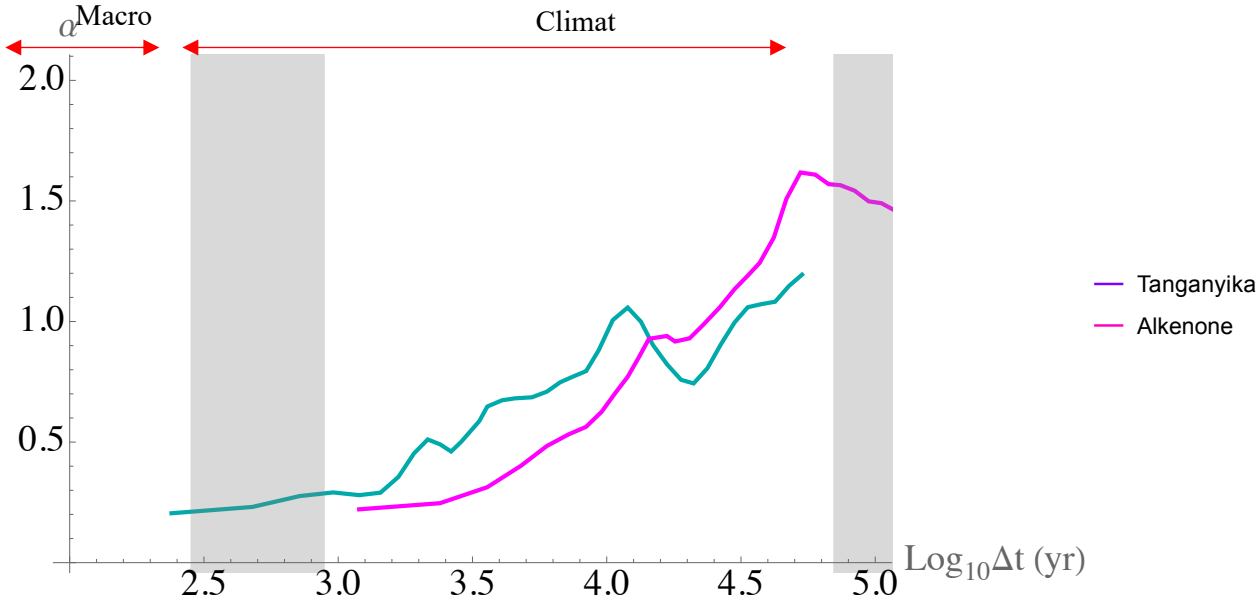

Figure S18: Estimates for the multifractal index α as a function of timescale for marine sediment datasets that measured temperature over the Quaternary. Transition scales between different climate regimes are shown by vertical grey bars. These datasets did not transition between scaling regimes, and no change in behaviour for α is observed. Instead, α is seen to steadily increase for all timescales.

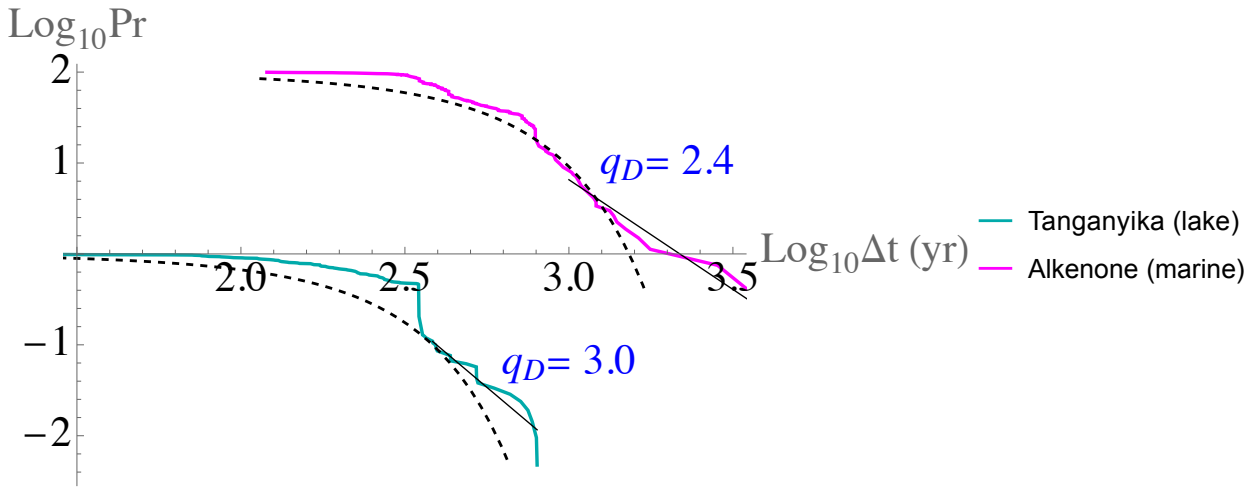

Figure S19: the probability distribution $Pr(\Delta\tau' > \Delta\tau)$ of intervals between consecutive datapoints in paleo chronologies from lake and marine sediment datasets that measured temperature over the Quaternary, where $\Delta\tau'$ is the duration of a random interval and $\Delta\tau$ is a threshold. Black dotted lines show the best fit Gaussian distribution, whereas straight black lines show a best fit linear curve on a portion of the data. The exponents q_D are shown for the linear log-log fits, where $Pr \approx \Delta\tau^{-q_D}$. Distributions have been offset vertically for presentation. A Gaussian fit does not describe either dataset well and both datasets have linear tails demonstrating scaling behaviour in the probability distribution.

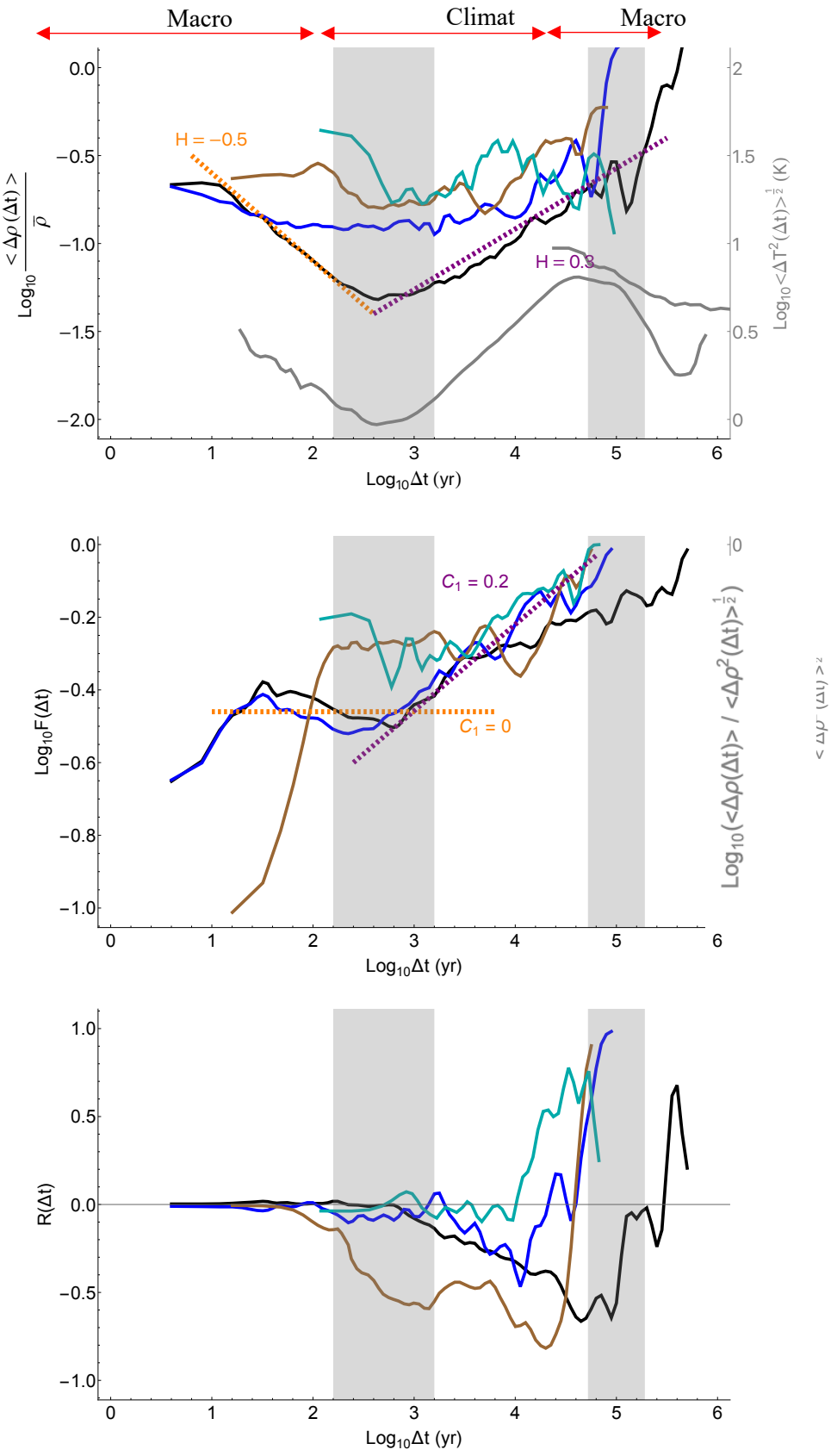
Macro
Climat
Macro
H = −0.5
H = 0.3
$\mathrm{Log}_{10}\frac{<\Delta\rho(\Delta t)>}{\bar{\rho}}$
$\mathrm{Log}_{10}<\Delta T^2(\Delta t)>^{\frac{1}{2}}$ (K)
$\mathrm{Log}_{10}\Delta t$ (yr)
C_1 = 0.2
C_1 = 0
$\mathrm{Log}_{10}F(\Delta t)$
$\mathrm{Log}_{10}(<\Delta\rho(\Delta t)> / <\Delta\rho^2(\Delta t)>^{\frac{1}{2}})$
$<\Delta\rho^2(\Delta t)>^{\frac{1}{2}}$
R(Δt)
EDC
Talos
NGRIP
RECAP

Figure S20: The results of Haar analysis on ice core datasets that measured dust concentrations over the Quaternary. a) $< \rho(\Delta t) >$, the slope of which gives an estimate of H, b) plot of log $F(\Delta t)$, the slope of which gives an estimate of C_1, and c) the correlation coefficient between fluctuations in measurement density and fluctuations in the measured quantity. In grey in plot a) are the fluctuations in temperature for the EDC (left) and Grossman (right) datasets to demonstrate the different scaling regimes of the climate system. The transition scales between different climate regimes are shown by vertical grey bars. Two distinct scaling regimes can be seen for each dataset: one with $H \approx -0.5$ and $C_1 \approx 0$ (fluctuating sedimentation rate dominant) and a second with $H \approx 0.3$ and $C_1 \approx 0.2$ (erosion process dominant). The transition timescale appears to be around 300 yr.

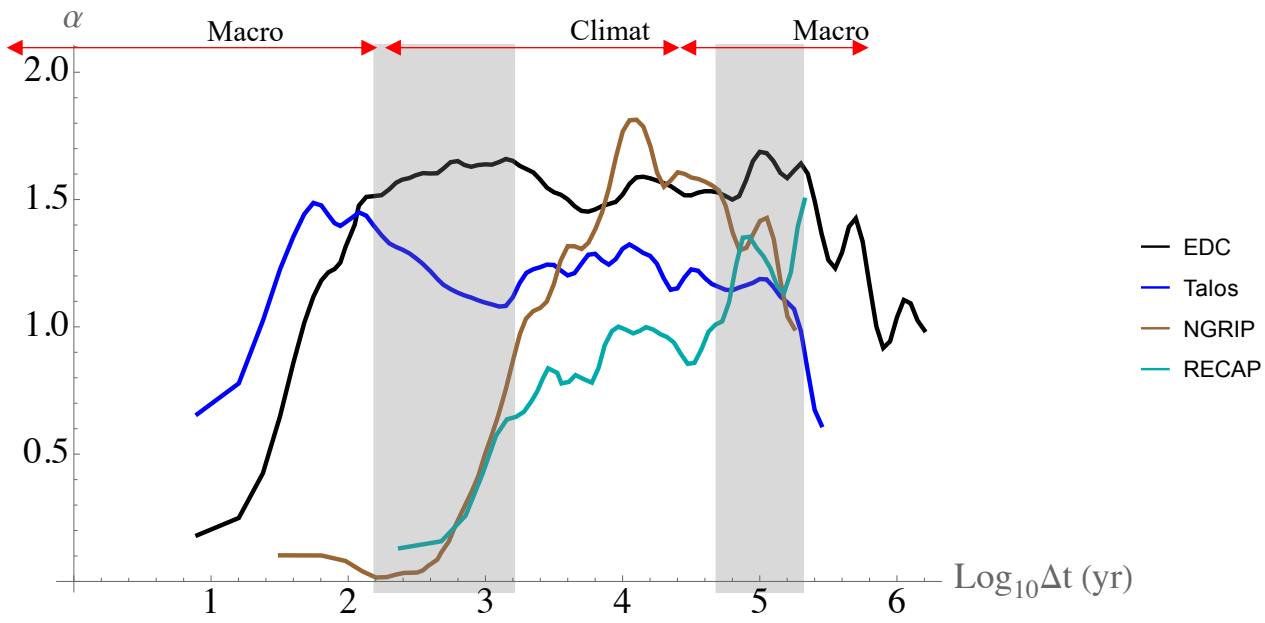

Figure S21: Estimates for the multifractal index α as a function of timescale for ice core datasets that measured dust concentrations over the Quaternary. The transition scales between different climate regimes are shown by vertical grey bars. At short timescales, $\alpha \approx 0$, but it undergoes a rapid increase - at the same timescale at which the scaling regime changes - to reach a plateau of $1 \lesssim \alpha \lesssim 1.5$ at longer timescales. This shows that at short timescales, the measurement density approaches a monofractal set, whereas at longer timescales it appears more as a multifractal. α for the NGRIP dataset does appear to decrease steadily after an initial peak at the transition timescale, however α remains much larger than at the very shortest timescales. This suggests that α does not remain in the range $1 \lesssim \alpha \lesssim 1.5$ indefinitely.

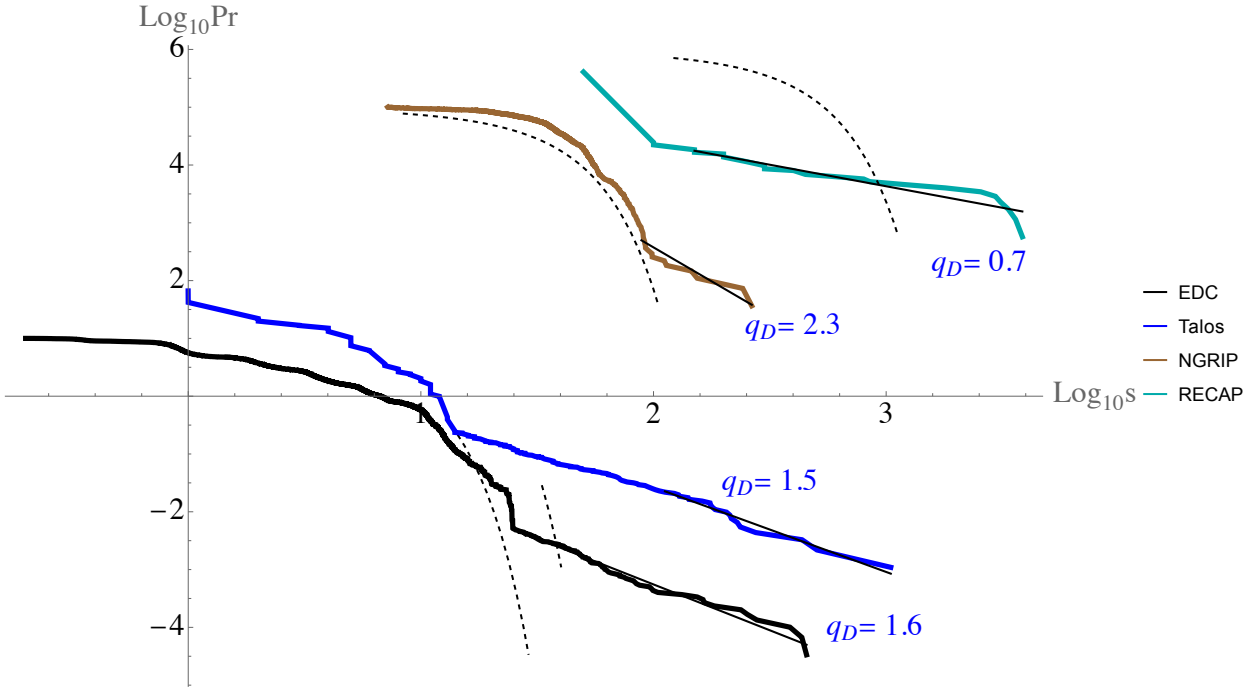

Figure S22: the probability distribution $Pr(\Delta\tau' > \Delta\tau)$ of intervals between consecutive datapoints in paleo chronologies from ice core datasets that measured dust concentration over the Quaternary, where $\Delta\tau'$ is the duration of a random interval and $\Delta\tau$ is a threshold. Black dotted lines show the best fit Gaussian distribution, whereas straight black lines show a best fit linear curve on a portion of the data. The exponents q_D are shown for the linear log-log fits, where $Pr \approx \Delta\tau^{-q_D}$. Distributions have been offset vertically for presentation. A Gaussian fit does not describe any dataset well, except for the start of the Talos distribution. However, all datasets have long linear tails, demonstrating scaling behaviour in the probability distribution.

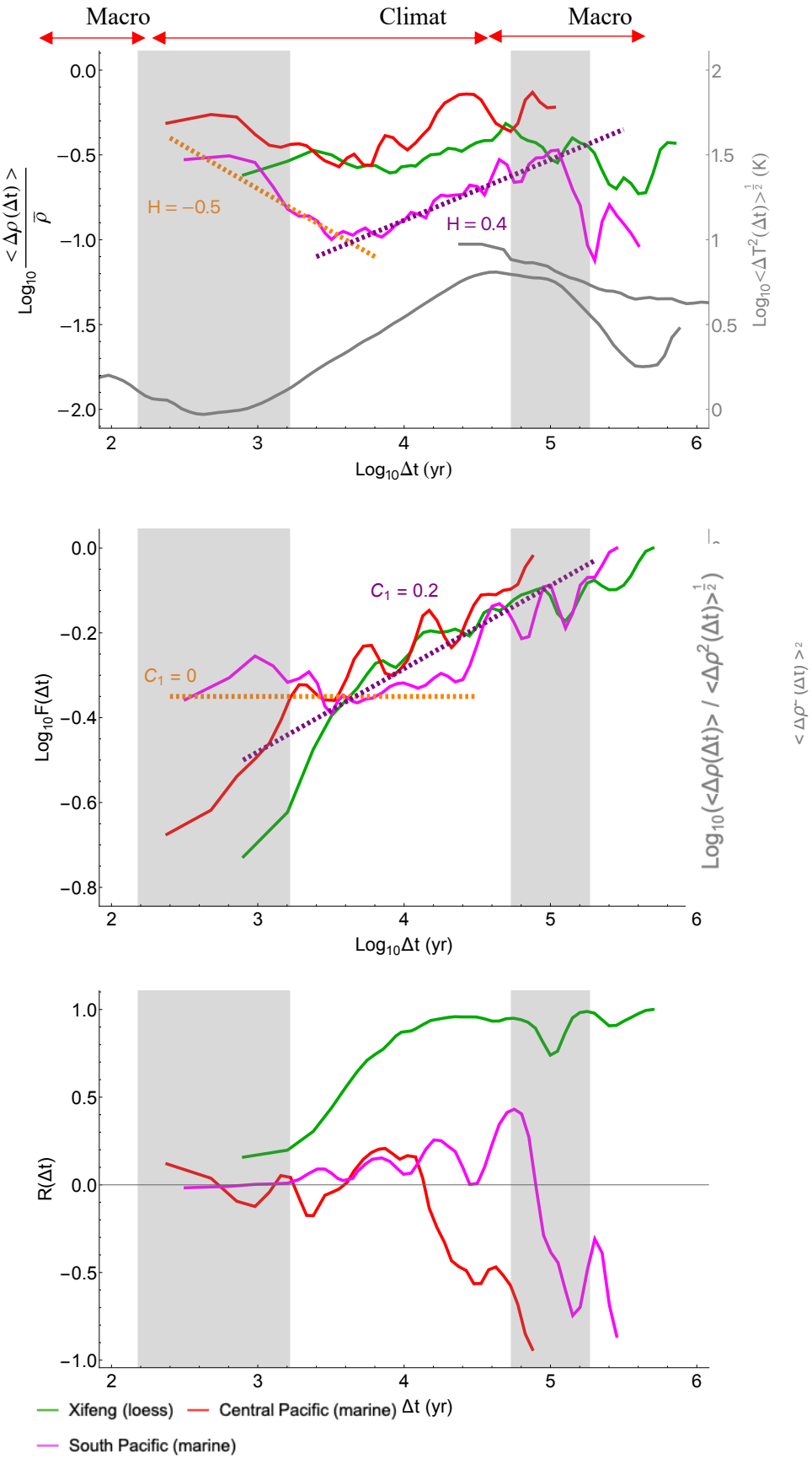
Macro
Climat
Macro
H = −0.5
H = 0.4
$\mathrm{Log}_{10}\frac{<\Delta\rho(\Delta t)>}{\bar{\rho}}$
$\mathrm{Log}_{10}<\Delta T^2(\Delta t)>^{\frac{1}{2}}$ (K)
$\mathrm{Log}_{10}\Delta t$ (yr)
C_1 = 0.2
C_1 = 0
$\mathrm{Log}_{10}F(\Delta t)$
$\mathrm{Log}_{10}(<\Delta\rho(\Delta t)> / <\Delta\rho^2(\Delta t)>^{\frac{1}{2}})$
$<\Delta\rho^n(\Delta t)>^2$
$\mathrm{Log}_{10}\Delta t$ (yr)
R(Δt)
Δt (yr)
Xifeng (loess)
Central Pacific (marine)
South Pacific (marine)

Figure S23: The results of Haar analysis on loess and marine sediment datasets that measured dust concentrations over the Quaternary. a) $< \rho(\Delta t) >$, the slope of which gives an estimate of H, b) plot of log $F(\Delta t)$, the slope of which gives an estimate of C_1, and c) the correlation coefficient between fluctuations in measurement density and fluctuations in the measured quantity. In grey in plot a) are the fluctuations in temperature for the EDC (left) and Grossman (right) datasets to demonstrate the different scaling regimes of the climate system. The transition scales between different climate regimes are shown by vertical grey bars. Two distinct scaling regimes can be seen for each dataset: one with $H \approx -0.5$ meaning that the measurement density is converging to a well-defined mean and a second with $H \approx 0.4$ meaning there is no well-defined sampling rate. The transition timescale between the two regimes is about 3000 yr. However, the scaling regimes are much less clear in the plots in b). Only the scaling regimes for the South Pacific dataset are clear in b) where $C_1 \approx 0$ in the first and $C_1 \approx 0.2$ in the second. However, for the other two datasets, $C_1 \approx 0.2$ at all time scales, suggesting that erosion processes were significant at all timescales for these datasets.

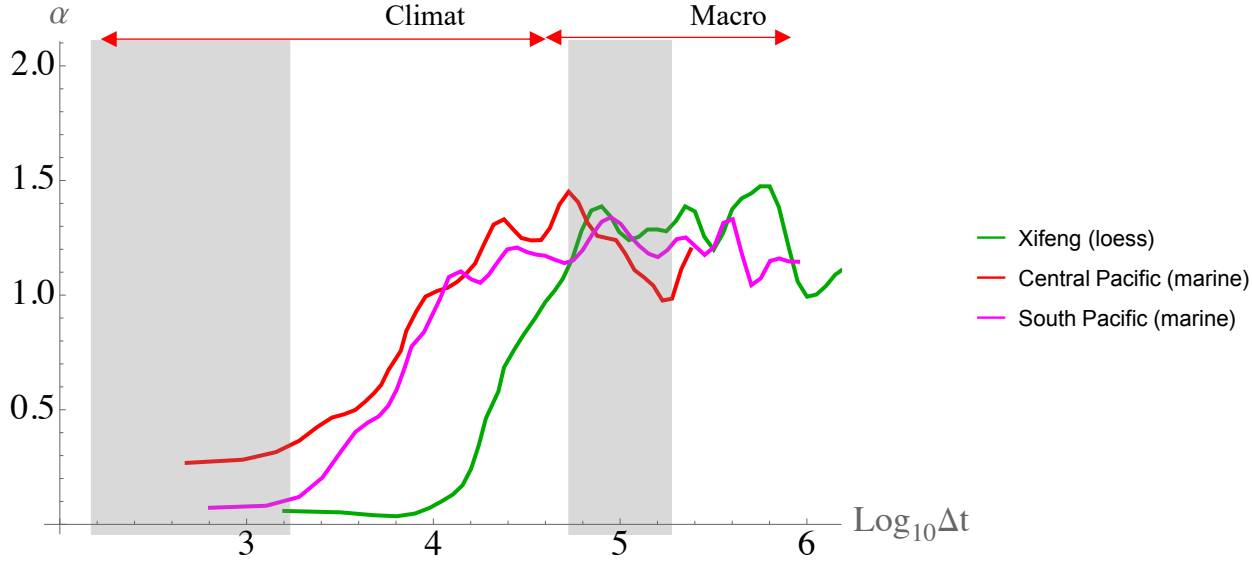

Figure S24: Estimates for the multifractal index α as a function of timescale for loess and marine sediment datasets that measured dust concentrations over the Quaternary. The transition scales between different climate regimes are shown by vertical grey bars. At short timescales, $\alpha \approx 0$, but it undergoes a rapid increase - at the same timescale at which the scaling regime changes - to reach a plateau of $1 \lesssim \alpha \lesssim 1.5$ at longer timescales. This shows that at short timescales, the measurement density approaches a monofractal set, whereas at longer timescales it appears more as a multifractal.

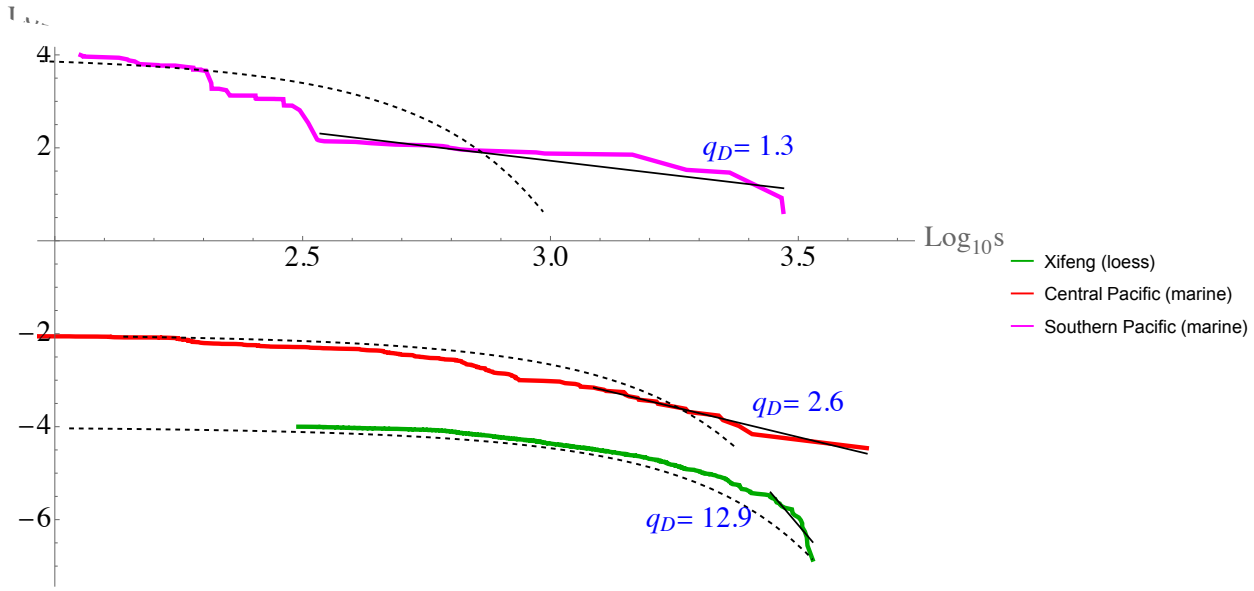

Figure S25: the probability distribution $Pr(\Delta\tau' > \Delta\tau)$ of intervals between consecutive datapoints in paleo chronologies from loess and marine sediment datasets that measured dust concentration over the Quaternary, where $\Delta\tau'$ is the duration of a random interval and $\Delta\tau$ is a threshold. Black dotted lines show the best fit Gaussian distribution, whereas straight black lines show a best fit linear curve on a portion of the data. The exponents q_D are shown for the linear log-log fits, where $Pr \approx \Delta\tau^{-q_D}$. Distributions have been offset vertically for presentation. A Gaussian fit describes the beginning of the Xifeng and Central Pacific datasets well, but all datasets have long linear tails for larger gaps, demonstrating scaling behaviour in the probability distribution.

Removal of large timescale trends

The statistical analyses estimate fluctuations at a given lag Dt by averaging over all the disjoint intervals of length Dt, the underlying assumption being that the series are statistically stationary. While this is a reasonable approximation for many of the series ti clearly is problematic for ice cores where even though (snow) sedimentation rates may be stationary, the lower parts of the core are significantly compressed due to the weight of the overlying ice. In this case, the series are clearly not stationary, yet it is straightforward to largely eliminate the effect by removing an overall linear or quadratic trend. Fig. 26 shows the result of this on the EDC series. Since the compression is a low frequency effect, as expected, the short lag statistics are essentially unaffected and the qualititative and even quantitative conclusions are essentially unchanged.

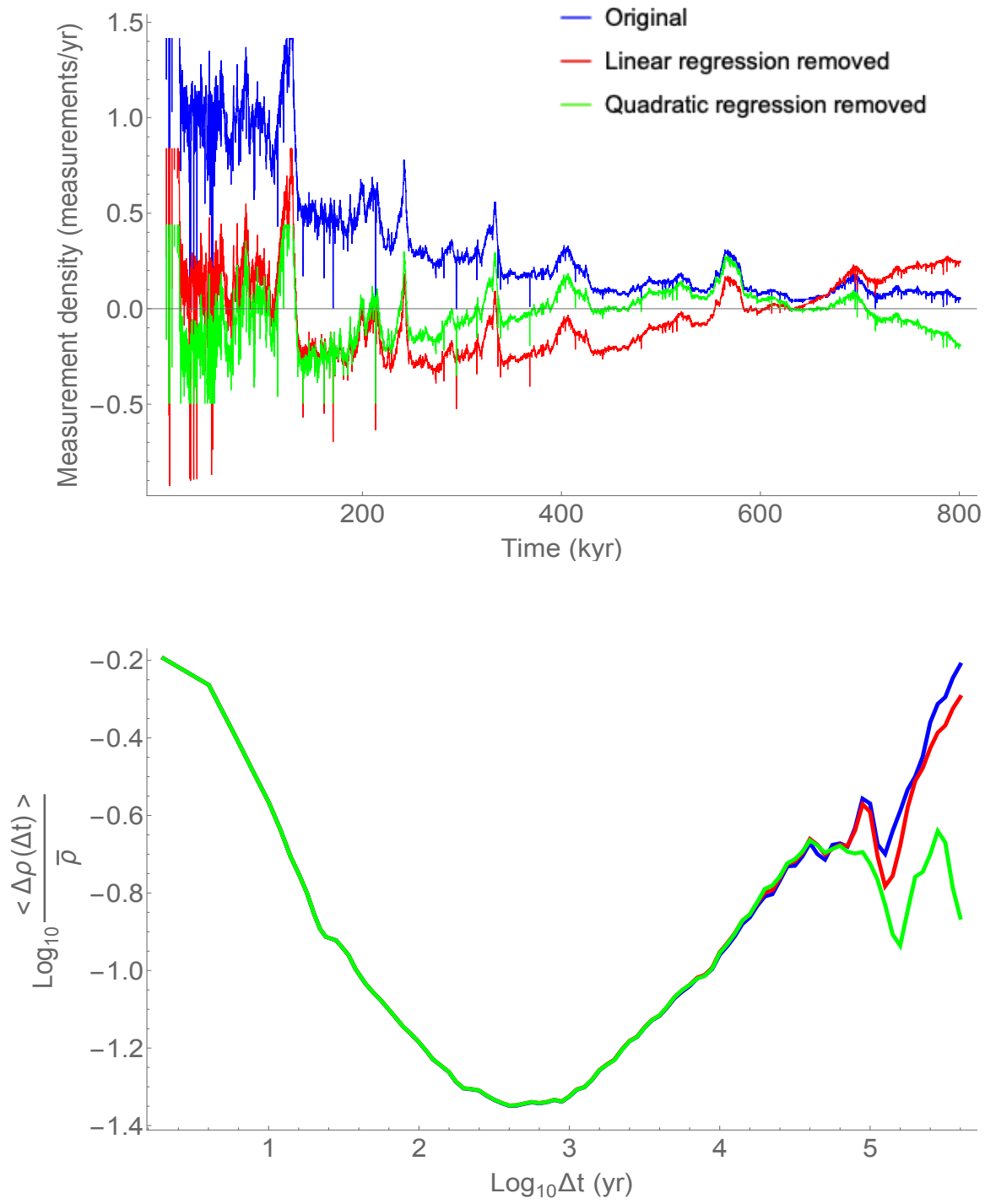

Figure S26: The measurement density of the EDC dataset, an ice ore that measured dust concentrations over the Quaternary as a function of the age of the sediment, with the temporal resolution degraded by a factor of 100 (top) and $< \rho(\Delta t) >$, the slope of which gives an estimate of H (bottom). These

plots are shown with the original measurement densities taken from the dataset (blue), the measurement densities with a linear regression removed (red), and with a quadratic regression removed (green). This was done to simulate the compression that the sediment undergoes over time due to pressure. By removing this compressive factor, it is possible to see that $< \rho(\Delta t) >$ is not strongly affected by this process except at the very lowest frequencies. Therefore, the compression of sediments does not seem to affect the conclusions drawn in this paper about the scaling regimes.